Minoia, S.; Carbonell, A.; Di Serio, F.; Gisel, A.; Carrinton, JC.; Navarro, B.; Flores Pedauye, R. (2014). Specific Argonautes Selectively Bind Small RNAs Derived from Potato Spindle Tuber Viroid and Attenuate Viroid Accumulation In Vivo. Journal of Virology. 88(20):11933-11945. https://doi.org/10.1128/JVI.01404-14

Specific ARGONAUTES bind selectively small RNAs derived from potato spindle tuber viroid and attenuate viroid accumulation *in vivo*

Sofia Minoia[1], Alberto Carbonell[2], Francesco Di Serio[3], Andreas Gisel[4], James C. Carrington[2], Beatriz Navarro[3]*, and Ricardo Flores[1]*

[1]Instituto de Biología Molecular y Celular de Plantas (IBMCP), Universidad Politécnica de Valencia-Consejo Superior de Investigaciones Científicas, Valencia, Spain, [2]Donald Danforth Plant Science Center, St. Louis, Missouri, USA, [3]Istituto per la Protezione Sostenibile delle Piante, Consiglio Nazionale delle Ricerche, Bari, Italy and [4]Istituto di Tecnologie Biomediche, Consiglio Nazionale delle Ricerche, Bari, Italy

Authors for correspondence:
Ricardo Flores
E-mail: rflores@ibmcp.upv.es Phone: 34-963877861 Fax: 34-963877859
Beatriz Navarro
E-mail: b.navarro@ba.ivv.cnr.it Phone: 39-0805443071 Fax: 39-080544 2911

Keywords: Argonaute proteins, dicer-like enzymes, small interfering RNAs, RNA silencing, viroids

Running title: Role of argonaute proteins on viroid infection

Word count for the abstract: 245

Word count for the text (excluding the references, table footnotes, and figure legends): 6432

ABSTRACT

The identification of viroid-derived small RNAs (vd-sRNAs) of 21-24 nucleotides (nt) in plants infected by viroids (infectious non-protein-coding RNAs of just 250-400 nt), supports their targeting by dicer-like enzymes, the first host RNA silencing barrier. However, whether viroids, like RNA viruses, are also targeted by the RNA-induced silencing complex (RISC) remains controversial. At the RISC core is one Argonaute (AGO) protein that, guided by endogenous or viral sRNAs, targets complementary RNAs. To examine whether AGO proteins also load vd-sRNAs, leaves of *Nicotiana benthamiana* infected by potato spindle tuber viroid (PSTVd) were agroinfiltrated with plasmids expressing epitope-tagged versions of AGO1, AGO2, AGO3, AGO4, AGO5, AGO6, AGO7, AGO9 and AGO10 from *Arabidopsis thaliana.* Immunoprecipitation analyses of the agroinfiltrated halos revealed that all AGOs, except AGO6, AGO7 and AGO10, associated with vd-sRNAs: AGO1, AGO2 and AGO3 preferentially with those of 21 and 22 nt, while AGO4, AGO5 and AGO9 additionally bound those of 24 nt. Deep sequencing analyses showed that sorting of vd-sRNAs into AGO1, AGO2, AGO4 and AGO5 depended essentially on their 5′-terminal nucleotide, with the profiles of the corresponding AGO-loaded vd-sRNAs adopting specific hot spot distributions along the viroid genome. Furthermore, agroexpression of AGO1, AGO2, AGO4 and AGO5 on PSTVd-infected tissue attenuated the level of the genomic RNAs, suggesting that they, or their precursors, are RISC-targeted. In contrast to RNA viruses, PSTVd infection of *N. benthamiana* did not affect miR168-mediated regulation of the endogenous AGO1, which loaded vd-sRNAs with specificity similar to its *A. thaliana* counterpart.

IMPORTANCE

To contain invaders, particularly RNA viruses, plants have evolved an RNA silencing mechanism relying on the generation by Dicer-like (DCL) enzymes of virus-derived

small RNAs of 21-24 nucleotides (nt) that load and guide Argonaute (AGO) proteins to target and repress viral RNA. Viroids, despite their minimal genomes (non-protein-coding RNAs of only 250-400 nt), infect plants and incite diseases. The accumulation in infected plants of 21-24 nt viroid-derived small RNAs (vd-sRNAs) supports that DCLs also target viroids, but does not clarify whether vd-sRNAs can activate one or more AGOs. Here, we show that in leaves of *Nicotiana benthamiana* infected by potato spindle tuber viroid, the endogenous AGO1 and distinct AGOs from *Arabidopsis thaliana* that were overexpressed, associated with vd-sRNAs displaying the same properties (5′-terminal nucleotide and size) previously established for endogenous and viral small RNAs. Overexpression of AGO1, AGO2, AGO4 and AGO5 attenuated viroid accumulation, supporting their role in antiviroid defense.

Viroids, regardless of having minimal genomes restricted to a single-stranded (ss) non-protein-coding RNA of solely ~250-400 nucleotides (nt), can parasitize the higher plants they infect and replicate, spread systemically, and frequently incite disease (1 to 3). Most of the approximately 30 viroids characterized so far, including the type species potato spindle tuber viroid (PSTVd) (4, 5), have been assigned to the family *Pospiviroidae* on the basis of a rod-like (or quasi-rod-like) secondary structure with a central conserved region (CCR), and replication in the nucleus through an asymmetric rolling-circle mechanism with double-stranded RNA (dsRNA) intermediates (6 to 10). This mechanism is catalyzed by the RNA polymerase II forced to transcribe RNA templates (11 to 13), an RNase most likely of class III (14), and the DNA ligase 1 redirected to act as an RNA ligase (15), with the CCR playing a critical role in the cleavage of the oligomeric (+) strands generated by the rolling circle-mechanism (14) and in the ligation (circularization) of the resulting monomeric (+) strands (16). The remaining four viroids, members of the family *Avsunviroidae*, display a quasi-rod-like or clearly branched secondary structure without CCR but with hammerhead ribozymes in both polarity strands; these catalytic RNA motifs mediate self-cleavage of the oligomeric strands produced by a symmetric rolling-circle mechanism occurring in plastids, mostly chloroplasts (17). To complete their infectious cycle, viroids must move at short (cell-to-cell) and long distance through the plasmodesmata and phloem, respectively. Some of the RNA motifs that mediate these movements have been finely dissected for PSTVd and include trafficking from the bundle sheath to mesophyll (18), entry of PSTVd from non-vascular into phloem tissue (19), and trafficking from palisade mesophyll to spongy mesophyll (20). A genome-wide mutational analysis has mapped loops/bulges in the secondary structure of PSTVd, crucial or relevant for replication in single cells (protoplasts) or for systemic movement (21).

In addition to replicate and move, viroids need to overcome their host surveillance responses, salient among which is RNA silencing (22, 23). This regulatory mechanism, which functions at the transcriptional and post-transcriptional level and

is particularly sophisticated in plants, tunes endogenous gene expression and plays a defensive role restricting pathogen invasion and transposon proliferation. The key elicitors of RNA silencing, dsRNAs and snap-folded ssRNA, are processed by specific Dicer-like (DCL) isozymes into small RNAs (sRNAs), mainly small interfering RNAs (siRNAs) of 21, 22 and 24 nt, ~~or~~ and microRNAs (miRNAs) of 21 and 22 nt (24, to 26). One strand of these sRNAs, and of some secondary siRNAs resulting from an amplification pathway catalyzed by endogenous RNA-directed RNA polymerases (RDRs) and DCLs (27, 28), preferentially loads and guides the RNA-inducing silencing complex (RISC), particularly its core consisting of an Argonaute (AGO) protein, to target and inactivate their cognate RNAs or DNAs (29).

Arabidopsis thaliana contains 10 AGO proteins classified in three clades: i) AGO1, AGO5, and AGO10, ii) AGO2, AGO3, and AGO7, and iii) AGO4, AGO6, AGO8, and AGO9. This phylogenetic grouping, however, does not necessarily imply functional similarity (29, 30). AGO1, AGO2, and AGO7 associate with 21- or 22-nt sRNAs (and AGO5 additionally with 24-nt sRNAs), either endogenous or exogenous (as those derived from viruses), and at least AGO1, AGO2 and AGO5 operate in post-transcriptional silencing through cleavage or translation arrest of their RNA targets (31 to 37). AGO4, AGO6, and AGO9 associate with 24-nt siRNAs to mediate transcriptional silencing through RNA-directed DNA methylation (38, 39), and at least AGO4 binds to diverse classes of sRNAs including siRNAs originating from transposable and repetitive elements, and cleaves target RNA transcripts (40). AGO10 acts in the translational control of several miRNA targets, like the mRNAs coding for AGO1 (41, 42). Finally, the role of AGO3 and AGO8 in sRNA-directed regulation remains unclear (29, 30). A recent transcriptome assembly has identified in *N. benthamiana* homologues for each AGO from *A. thaliana,* except for AGO3 and AGO9 (returned as AGO2 and as a variant of AGO4, respectively) (43).

Several independent lines suggest that, in addition to playing a key role in antiviral defense, RNA silencing is also involved in antiviroid defense. First, viroid infection results in the genomic RNA progeny folding upon itself into collapsed

secondary structures and in the production of dsRNAs, either replicative intermediates or RDR products. Northern hybridizations have detected viroid-derived sRNAs (vd-sRNAs), with properties akin to the host and virus sRNAs generated by DCLs, accompanying infections by representative members of the two viroid families; these vd-sRNAs have been subsequently sequenced by conventional and high-throughput approaches (44, 45). Second, the expression of a reporter gene and the accumulation in infected plants of the genomic viroid RNA appears to be repressed by vd-sRNAs in a sequence-specific mode (46 to 49). Third, increased levels of the genomic PSTVd RNA have been detected in early infection stages of *Nicotiana benthamiana* deficient for RDR6, in which, additionally, PSTVd entry into floral and vegetative meristems is facilitated (50). Fourth, two vd-sRNAs containing the albinism determinant of a chloroplast-replicating viroid guide cleavage of the host mRNA coding for the chloroplastic heat-shock protein 90 (cHSP90) as predicted by RNA silencing, thus providing a feasible mechanism of pathogenesis (51). Fifth, the titer of a viroid is enhanced in co-infections with a virus, with this effect occurring via the expression of viral-encoded silencing suppressors (52). And, last but not least, early pioneering research discovered that PSTVd-cDNA introduced into the tobacco genome via *Agrobacterium tumefaciens* became methylated only following viroid RNA-RNA replication, thus unveiling an RNA-directed and sequence-specific mechanism for *de novo* methylation of genomic sequences in plants (53); this mechanism of transcriptional silencing is now known to be mediated by specific DCL-dependent siRNAs and AGOs. More recently, viroid infection has been associated with changes in DNA methylation of host ribosomal RNA genes (54), but whether those changes result from direct or indirect effects is not known. However, despite all these data, no direct evidence exists supporting that AGOs recruit vd-sRNAs. We report here that certain members of the AGO family, specifically AGO1, AGO2, AGO4 and AGO5 load vd-sRNAs from PSTVd, and eventually attenuate the viroid titer.

MATERIALS AND METHODS

PSTVd inoculation. *Nicotiana benthamiana* seedlings were grown in a controlled chamber (28°C with fluorescent light for 16 h and 25°C in darkness for 8 h) and, at the cotyledon/first true leaf stage, they were infiltrated with cultures of *Agrobacterium tumefaciens* C58 carrying a binary plasmid empty or with a head-to-tail dimeric insert of PSTVd (NB variant, GenBank accession number AJ634596.1) under the control of the 35S promoter of cauliflower mosaic virus (CaMV) (55).

Agroinfiltration assays. Binary plasmids for expressing, under the control of the 35S promoter of CaMV, AGO versions from *A. thaliana* tagged at their N-terminal region with three tandem repeats of the HA epitope (AGO1, AGO2, AGO7 and AGO10), or with a single HA epitope (AGO3, AGO4, AGO5, AGO6 and AGO9), were described previously (34, 37). Binary plasmids for expressing miR390 from *A. thaliana* and the beta-glucuronidase (GUS) from *Escherichia coli,* both under the control of the 35S promoter of CaMV, were also described previously (34). Transient expression assays in *N. benthamiana* leaves with cultures of *A. tumefaciens* were performed as described previously (56, 57).

RNA extraction and analysis by PAGE and Northern-blot hybridization. Total RNA preparations (RNA-Input) or immunoprecipitates (RNA-IP, see below) from PSTVd-infected upper non-inoculated leaves of *N. benthamiana* (and from mock-inoculated controls) were obtained by double extraction with buffer-saturated phenol, precipitated with ethanol, and resuspended. RNAs were then separated by denaturing PAGE (in 1X TBE buffer and 8 M urea) on either 5% gels (for the monomeric circular, *mc,* and linear, *ml,* PSTVd forms) or 17% gels (for vd-sRNAs and miRNAs) that were stained with ethidium bromide for assessing equal loading by the fluorescence emitted by the 5S or 4S RNAs. Following electrotransference of RNAs to Hybond-N+ membranes (Roche Diagnostics GmbH), they were hybridized with internally-radiolabeled full-length riboprobes (synthesized by *in vitro* transcription) for detecting PSTVd (+) strands, or with 5'-radiolabeled deoxyribonucleotide probes [prepared according to standard procedures (58)] for detecting specific miRNAs.

Hybridization was at 70°C in the presence of 50% formamide (for detecting *mc* and *ml* forms), or at 42°C with PerfectHyb Plus hybridization buffer (Sigma) (for detecting vd-sRNAs) (50). After washing at 60°C in 0.1X SSC with 0.1% SDS (*mc* and *ml* forms), or at 55°C in 1X SSC with 0.1%SDS (vd-sRNAs and miRNAs), the membranes were analyzed with a phosphoimager (Fujifilm FLA-5100) using programs Image Reader FLA-5100 and Image Gauge 4.0.

RNA Immunoprecipitation assays. RNA-IP were obtained with a rabbit polyclonal antibody (GenScript) against the N-terminal region of AGO1 from *N. benthamiana* (MVRKKRTDVPGGAESFESHEC), which is characteristic of this AGO isoform, and with a mouse monoclonal antibody (12CA5, Roche Diagnostics GmbH) against an epitope of the hemaglutinin (HA) from human influenza virus. Immunoprecipitation assays were performed as reported previously (37) with minor modifications. In brief, *N. benthamiana* leaves (0.5-1 g) were homogenized with liquid nitrogen and mixed with 12 ml/g (HA antibody) or 3 ml/g (AGO1 antibody) of lysis buffer [50 mM Tris-HCl, pH 7.4, 2.5 mM $MgCl_2$, 100 mM KCl, 0.1% Nonidet P-40, 1 μg/ml leupeptin, 1 μg/ml aprotonin, 0.5 mM phenylmethylsulfonyl fluoride, and one tablet of complete proteinase inhibitor cocktail (Roche Diagnostics GmbH)]. The insoluble material was removed by centrifugation at 8000 X *g* for 5 min at 4°C and, after taking two aliquots (of 20 μl and 1 ml) for analysis of the Protein- and RNA-Input fractions, respectively, the remaining clarified lysate was incubated at 4°C for 15 min with 4 μg/ml of one (HA) or the other (AGO1) antibody, and then at 4°C for 30 min with 100 μl/ml of Protein-A agarose beads (Roche Diagnostics GmbH). Beads were washed six times for 10 min with lysis buffer at 4°C and, after taking one aliquot (20 μl) of the final bead suspension for Protein-IP analysis, the rest was used for RNA-IP analysis. RNAs were released by incubating the beads at 65°C for 15 min in 0.5 vol of proteinase K buffer [0.1 M Tris-HCl, pH 7.4, 10 mM EDTA, 300 mM NaCl, 2% SDS, and 1 μg/μl proteinase K (Roche Diagnostics GmbH)]. RNA-Input and RNA–IP aliquots were extracted with saturated phenol pH 4.5 (Amresco), phenol:chloroform:isoamyl alcohol, and chloroform, and recovered by ethanol precipitation. For sRNA gel blot assays, 2-5 μg

of RNA of the RNA-Input fraction, and one half of the RNA-IP fraction, were used as indicated in the previous section. For protein blot assays, 20 µl of the Protein-Input and Protein-IP fractions were mixed with the same volume of 2X PDB buffer (1.25 M Tris pH 6.8, 10% SDS, 80% glycerol, 10% β-mercaptoetanol and 0.02% bromophenol blue) and heated at 100°C for 3 min; aliquots (10 and 2.5 µl, respectively) were applied onto NuPAGE Bis-Tris minigels (4-12%) (Novex, Life Technologies) and equal loading was assessed by the intensity generated by the large subunit of Rubisco after staining with Ponceau S (Sigma). HA-AGOs were electrotransferred to PVDF membranes and detected by chemiluminescence with anti-HA peroxidase antibody (Roche Diagnostics GmbH) at a 1:1000 dilution and Western Lighting plus-ECL substrate (Perkin-Elmer). AGO1 from *N. benthamiana* was similarly detected, but using the antibody against its N-terminal region at a 1:1000 dilution and a goat anti-rabbit IgG (H&L) secondary antibody conjugated to horse radish peroxidase (Agrisera) at a 1:20000 dilution, and the same substrate.

Deep sequencing analysis of sRNAs. Experimental details on sRNA purification, adapter ligation, RT-PCR amplification, library purification, and high-throughput DNA sequencing on the Illumina Genome Analyzer Hi-Seq 2000 (FASTERIS SA, Plan-les-Ouates, Switzerland), has been described previously (50). In the first deep sequencing four bar-coded samples, corresponding total sRNAs (inputs) and immunoprecipitates (IPs, obtained with an anti-HA monoclonal antibody) from PSTVd-infected *N. benthamiana* overexpressing HA-tagged AGO1 and -AGO2, were run in the same channel. In the second deep sequencing we proceeded as in the first, but the four bar-coded samples corresponded to sRNAs inputs and IPs from PSTVd-infected *N. benthamiana* overexpressing HA-tagged AGO4 and -AGO5. In the third deep sequencing, we proceeded again as in the first, but the four bar-coded samples corresponded to sRNAs inputs and IPs (obtained with an anti-AGO1 polyclonal antibody) from mock-inoculated and PSTVd-infected *N. benthamiana*. The resulting reads, after bar-code identification, were processed by removing the adaptor and grouping them into different files according to their sequence length. Only 18-26 nt

reads were mapped against the PSTVd sequence (variant NB) (59). To filter, analyze and visualize the mapping data, a set of perl scripts was developed. IP enrichment or depletion was calculated for each unique 21-, 22- or 24-nt vd-sRNA as log2 [(IP reads + 1)/(Input reads +1)], and plotted for each size class as the fraction (%) of unique vd-sRNA sequences enriched >2-fold (log2 >1) or depleted >2-fold (log2<1) in the IP compared to the input.

RESULTS

PSTVd infection of *N. benthamiana* does not affect miR168-mediated AGO1 accumulation. As indicated above, AGO1 is a key player of the antiviral defense mediated by RNA silencing. Infection by plant RNA viruses induces and reduces the accumulation of AGO1 mRNA and AGO1 protein, respectively (42, 60). The explanation for this apparent paradox is that expression of AGO1 mRNA is translationally repressed by miRNA168 (61), the accumulation of which is elicited by virus infection (42, 60). In view of these results, we first checked whether a similar situation occurs during a viroid infection. For this purpose, plants of *N. benthamiana* were inoculated by leaf infiltration with cultures of *A. tumefaciens* carrying binary plasmids for expressing a head-to-tail dimeric (+) insert of PSTVd [*35S:dPSTVd(+)*] or the beta-glucuronidase (GUS) (*35S:GUS*), both under the control of the 35S promoter of CaMV. Western-blot analysis of PSTVd-infected upper non-inoculated leaves —using a polyclonal antibody raised specifically against the N-terminal region of AGO1 from *N. benthamiana*— revealed that infection by PSTVd induced a slight increase in the accumulation of AGO1 compared with mock-inoculated controls (expressing GUS) of the same developmental stage. This effect was observed in leaves collected at early (15 dpi, when symptoms start appearing) and later infection stages (20, 25 and 30 dpi) (Fig. 1A). However, no significant effect on AGO1 was detected when the leaves of *N. benthamiana* agroinfiltrated with the plasmid for expressing

the head-to-tail dimeric insert of PSTVd were directly examined at 4, 6 and 8 dpi (using again as control leaves agroinfiltrated with *35S:GUS*) (Fig. 1B).

Although these results anticipated that miRNA168 levels were most likely not affected by PSTVd infection, we confirmed that this was indeed the case examining total RNA preparations from the same samples by Northern-blot hybridization to detect miRNA168 (Fig. 1A and B). Altogether our data showed that, in contrast with the situation observed for representative RNA viruses (42, 60), the effect of viroid infection on AGO1, if any, is not mediated by miRNA168 targeting of AGO1 mRNA.

Endogenous AGO1 loads vd-sRNAs during PSTVd infection of *N. benthamiana*. Using the polyclonal antibody against AGO1 from *N. benthamiana*, we next tested whether this protein interacts *in vivo* with vd-sRNA. Approximately three weeks after inoculation, plants displayed a stunted phenotype with curling and reduction of the foliar area when compared with the mock-inoculated controls, as reported previously for this and other PSTVd strains (50, 62). Analysis of total RNA preparations by denaturing PAGE (in 5% gels) and Northern-blot hybridization confirmed the accumulation of the monomeric circular *(mc)* and linear *(ml)* PSTVd (+) RNAs in upper non-inoculated leaves collected at 20, 25 and 30 days postinfiltration (dpi) (Fig. 1C). Parallel analysis of the same samples, fractionated by denaturing PAGE (in 17% gels), revealed intense hybridization signals in the gel region corresponding to vd-sRNAs of 21 to 24 nt (Fig. 1C). Moreover, a minor fraction of the vd-sRNAs of 21-22 nt were also detected in the immunoprecipitates generated by the AGO1-specific antibody (Fig. 1C), hence showing that the host AGO1 indeed interacts with PSTVd-sRNAs with the expected size specificity (29). A more detailed description of those PSTVd-sRNAs loaded by AGO1 from *N. benthamiana* is provided below.

Setting up a system for the study of AGO/vd-sRNA interactions: agroexpressed AGO1 and AGO2, but neither AGO7 nor AGO10, bind PSTVd-sRNAs. To circumvent the problem posed by the inability of PSTVd to infect *A. thaliana* (10) and by the lack of specific antibodies against most other AGOs from *N. benthamiana,* we then tested whether overexpressing AGO1 and other AGO members from *A. thaliana* in PSTVd-

infected *N. benthamiana* resulted in their loading with vd-sRNAs. To increase recovery in immunoprecipitates, we used AGO versions tagged at their N-terminal region with three tandem repeats of the HA epitope (AGO1, AGO2, AGO7 and AGO10) (34, 37), or with a single HA epitope (AGO3, AGO4, AGO5, AGO6 and AGO9, kindly provided by Drs. A. Takeda and Y. Watanabe). First we reproduced results obtained with a protocol reported previously showing that AGO7 and miR390 from *A. thaliana* interact specifically when overexpressed in *N. benthamiana* (34). On the one hand, leaves of non-infected *N. benthamiana* were agroinfiltrated with a culture of *A. tumefaciens* with the construct *35S:miR390* for expressing miR390 under the control of the 35S promoter. On the other hand, this same culture was coagroinfiltrated with others carrying plasmids for expressing either AGO1 or AGO7, both tagged with the HA epitope and under the control of the same promoter (*35S:HA-AGO1* and *35S:HA-AGO7*, respectively). Northern-blot hybridizations with a 5'-radiolabeled oligodeoxyribonucleotide complementary to miR390 revealed that while this RNA accumulated to high levels in the total RNA fraction from infiltrated halos, it was only detected in AGO7 immunoprecipitate (data not shown). Given that AGO7, but not AGO1, binds specifically miR390 (34), and that Western-blot analysis with an anti-HA-peroxidase monoclonal antibody showed similar accumulation of AGO1 and AGO7 in the total protein and in the immunoprecipitate fractions (data not shown), these results provided the support needed for extending the same approach to investigate whether one or more AGOs interact specifically with vd-sRNAs.

We initially examined AGO1, AGO2, AGO7 and AGO10 from *A. thaliana* because some of them have been involved in defense against RNA viruses, namely AGO1, AGO2 and AGO7 against turnip crinkle virus (TCV), AGO2 against turnip mosaic virus (TuMV) (37) and AGO1 and AGO2 against cucumber mosaic virus (CMV) (31, 33, 36), and also because they display distinct size and sequence specificity for some sRNAs (29, 30). Moreover, when the present work was started, association of AGO10 with sRNAs had not been shown (29), thus serving this protein as a non-sRNA- binding AGO control. To begin with, each plasmid for expressing the HA-tagged AGOs was

coagroinfiltrated with the *35S:dPSTVd(+)* construct to trigger infection. Analysis by denaturing PAGE and Northern-blot hybridization revealed the presence of vd-sRNAs in the total RNA fractions from the coagroinfiltrated halos —with higher intensity at three than at two dpi— but not in the corresponding immunoprecipitates (data not shown). In view of these results, we took an alternative approach: plants were first agroinfiltrated with the *35S:dPSTVd(+)* construct and 19 days later, when PSTVd had spread systemically, upper non-inoculated leaves were then agroinfiltrated with the HA-tagged AGO constructs (*35S:3xHA-AGO1*, *35S:3xHA-AGO2*, *35S:3xHA-AGO7* or *35S:3xHA-AGO10)*. Analysis as stated above of the corresponding halos at two days after the second agroinfiltration showed high accumulation of vd-sRNAs of 21 to 24 nt in the total RNA fractions of the four samples, in contrast with the immunoprecipitates, wherein only vd-sRNAs of 21-22 nt were detected and exclusively associated with AGO1 and AGO2 (Fig. 2A). Western-blot analyses showed that the four agoinfiltrated AGOs (AGO1, AGO2, AGO7 and AGO10) were expressed (Fig. 2A). Altogether, these results indicated that vd-RNAs behave like other sRNAs of viral and endogenous origin (29), being specifically loaded in some, but not in all, AGOs according mainly to their size (and possibly to other structural properties, see below).

Agroexpressed AGO3, AGO4, AGO5 and AGO9 also bind vd-sRNAs with different affinity. We then extended these analyses to other available constructs, also under the control of the 35S promoter, for expressing the single HA-tagged AGOs from *A. thaliana*: *35S:HA-AGO3*, *35S:HA-AGO4*, *35S:HA-AGO5*, *35S:HA-AGO6 a*nd *35S:HA-AGO9*; *35S:3xHA-AGO2* was used as an internal control for linking results from these experiments with those of the previous one. Analysis by denaturing PAGE and Northern-blot hybridization of the corresponding halos at two days after the second agroinfiltration revealed high levels of vd-sRNAs of 21, 22 and 24 nt in the total RNA fractions of all samples, except in a negative control in which the *35S:dPSTVd(+)* construct used in the first agroinfiltration for triggering PSTVd infection was replaced by the *35S:GUS* construct (Fig. 2B). However, the immunoprecipitate fractions

behaved in a different manner: the vd-sRNAs of 21-22 nt were detected in samples expressing AGO2 and AGO3, while in the samples expressing AGO4 and AGO5 (and to a lower extent in that expressing AGO9) vd-sRNAs of 24 nt were additionally detected; in contrast, essentially no vd-sRNAs were observed in the sample expressing AGO6 (Fig. 2B). Recovery of AGO-bound vd-sRNAs from immunoprecipitates could be influenced by the HA epitope being single or triple and by the distinct stability of AGOs against endogenous proteases, although Western-blot analyses with the anti-HA-peroxidase monoclonal antibody showed that, even if with different extension, all agroinfiltrated AGOs were expressed (Fig. 2B). AGO6 inability to bind vd-sRNAs was nevertheless confirmed in further experiments (data not shown). Collectively, these results are consistent with vd-RNAs being differentially sorted into specific AGOs according to the size reported previously for other viral and endogenous sRNAs (29, 30).

Deep sequencing reveals that sorting of vd-sRNAs into AGO1, AGO2, AGO4 and AGO5 mainly depends on their size and 5′-terminal nucleotide. To better understand the differential AGO affinity for vd-sRNAs, AGO1 and AGO2 (as representatives of those members of the family that associate preferentially with the sRNAs of 21-22 nt), and AGO4 and AGO5 (as representatives of those members of the family that associate additionally with the sRNAs of 24 nt) (29, 30), were selected for further examination. Moreover, while AGO1, AGO2 and AGO5 are able to bind virus-derived sRNAs and have been involved in antiviral defense presumably via post-transcriptional gene silencing (31, 33, 36, 37), AGO4 mostly mediates transcriptional silencing (38). Previous immunoprecipitation assays have also revealed that the identity of the 5′-terminal nucleotide and the length of the sRNAs contribute to their sorting into these four AGO proteins (34, 35, 63).

The first deep sequencing of sRNAs resulted in approximately 137.500.000 reads, 95.6% of which corresponding to the four bar-coded samples run in the same channel: the total sRNAs (inputs) and immunoprecipitates (IPs) from PSTVd-infected *N. benthamiana* overexpressing AGO1 and AGO2, with the fraction of each sample

representing 23-29% of the total number of reads. Within the range of 18-26 nt, vd-sRNAs amounted to about 22% in the inputs, and 34% and 53% in AGO1-IP and AGO2-IP, respectively. The second deep-sequencing of sRNAs generated roughly 209.300.000 reads, 96.6% of which corresponding to the four bar-coded samples run in the same channel: the inputs and IPs from PSTVd-infected *N. benthamiana* overexpressing AGO4 and AGO5, with the fraction of each sample representing 19-29% of the total number of reads. Within the range of 18-26 nt, vd-sRNAs amounted to 11-15% in the inputs, and 14% and 28% in AGO4-IP and AGO5-IP, respectively. Therefore, with respect to the inputs, the proportion of vd-sRNA was enriched in the IPs, making up a significant fraction of the total. This bias was also observed (particularly in AGO4 and AGO5) when the vd-sRNAs were disaggregated into size classes (Fig. 3).

Analysis of the vd-sRNA reads from the inputs revealed a similar size distribution in the four samples: 44-45% were of 21 nt, 36-38% of 22 nt, and 9-9.5 of 24 nt, in agreement with previous results (50). However, the situation was somewhat different in the IPs, dominated in AGO1 and AGO2 by vd-sRNAs of 21 and to a lower extent 22 nt (with those of 24 nt being essentially absent), while the preponderant vd-sRNA species in AGO4 and AGO5 were of 22 nt (and to a lower extent of 21 nt), with those of 24 nt amounting to 18 and 10%, respectively. Hence, the AGO proteins exert some size-based selection on the vd-sRNAs they capture. On the other hand, the bias between (+) and (-) vd-sRNAs (derived from the most and less abundant viroid strands accumulating *in vivo,* respectively) was minor in inputs and IPs, except in the AGO2-IP, wherein the fraction of vd-sRNAs of (+) polarity was significantly higher (data not shown).

We next compared the distribution of the vd-sRNAs with respect to their 5'-terminal nucleotide, considering that in Arabidopsis this feature has a crucial role in sorting the sRNAs into the different AGOs (34, 35, 63). While 21- and 22-nt vd-sRNAs with a 5'-terminal U and C were moderately predominant in the inputs (up to 37% and 33%, respectively), the corresponding IP patterns were highly biased in their 5'-

terminal nucleotides: 81% (U), 98% (A), 59% (A) and 72% (C) in AGO1, AGO2, AGO4 and AGO5, respectively (Fig. ~~5~~ 4). As for the 24-nt vd-sRNAs, those with a 5′-terminal G were moderately prevalent (33%) in the AGO4 input, as also were those with a 5′-terminal U or C in the AGO5 input (29%); yet, the distribution in their IP counterparts was clearly biased for vd-sRNAs with a 5′-terminal C, which were underrepresented in AGO4-IP (8%) but prevalent in AGO5-IP (77%). This result indicates that the strong preference of AGO5 for binding vd-sRNAs with a 5′-terminal C is size independent. Similar distributions were obtained when the (+) and (-) vd-sRNAs from the IPs were examined separately (data not shown). Altogether, these results support that the 5′-terminal nucleotide of vd-sRNAs is a major determinant for AGO sorting, following similar rules as those governing AGO sorting of endogenous and viral sRNAs (34, 35, 63). However, as proposed for certain endogenous sRNAs (39), characteristics other than the 5′-terminal nucleotide may also contribute to vd-sRNA loading.

The profiles of AGO-loaded vd-sRNAs adopt specific hot spot distributions along the viroid genome. Analysis of the vd-sRNA reads from AGO IPs revealed that they mapped at numerous positions of the genomic (+) and (-) viroid strands, with a significant fraction of the reads accumulating in specific regions (hot spots), and displaying some peculiarities (Fig. 5). First, the hot spot profiles of the vd-sRNAs immunoprecipitated by each of the four AGO tested were different, as a consequence of their affinity for specific 5′-terminal nucleotides and of the uneven distribution of the four nucleotides in the PSTVd (+) and (-) genomic strands. Yet, the IP profiles were not a direct reflection of their corresponding input counterparts (see for instance the vd-sRNAs with their 5′-terminal U mapping at positions ~240 and ~333 in the (+) strand, and ~123 and ~281 in the (-) strand, which are overrepresented in the AGO1 IP with respect to the AGO1 input), thus indicating the existence of some bias (Fig. ~~6~~ 5). Second, hot spots in both input and IP profiles mapped at regions with a high G+C content, a likely consequence of the preference of DCLs for such regions (64, 65). And third, focusing on the vd-sRNAs mapping around positions 45-50 and 308-318 of the pathogenic (P) domain, 119-122 in the limit between the central (C)

and variable (V) domains, and 257 and 259 of the C domain —all associated with pathogenesis (66, 67)— striking accumulation of those of (-) and (+) polarity around positions 119-122 were observed in the AGO1 and AGO2 IPs, respectively (Fig. ~~6~~ 5). This result may have implications on the mechanism of symptom induction, despite the observation that low-abundant vd-sRNAs can be functionally relevant (see Discussion).

Agroexpression of AGO1, AGO2, AGO4 and AGO5 on PSTVd-infected tissue attenuates the level of the genomic RNAs. To test whether AGO-loaded vd-sRNAs could have a functional effect, we next examined the titer of the *mc* and *ml* PSTVd (+) forms. For this purpose, plants of *N. benthamiana* were agroinfected with PSTVd as indicated previously and, eight days later, upper non-inoculated leaves were agroinfiltrated with *A. tumefaciens* cultures for expressing HA-AGO1 or HA-AGO2; total RNA preparations from the corresponding halos were extracted two days afterward. Subsequent to some preliminary experiments, we chose this early sampling time to avoid that the potential effects of AGOs could be masked at later infectious stage, when the accumulation levels of the genomic viroid RNA increase very rapidly. Plants of *N. benthamiana* agroinfiltrated with cultures for expressing HA-AGO7 and GUS, as well as mock-inoculated plants, were included as controls based on previous results (Fig. 2). Analysis by denaturing PAGE and Northern-blot hybridization showed that the titer of *mc* and *ml* PSTVd (+) RNAs in plants expressing HA-AGO1 and HA-AGO2 was lower than that of the controls expressing HA-AGO7 and GUS (Fig. 6A). Similar effects (attenuation of the titer of *mc* and *ml* PSTVd (+) RNAs with respect to the same controls) were observed in plants expressing HA-AGO4 and HA-AGO5 (Fig. 6B). These results are consistent with the view that AGO1, AGO2, AGO4 and AGO5, loaded with vd-sRNAs and forming part of RISC, target PSTVd RNAs. Thus, not only DCLs —as revealed by the generation of vd-sRNAs in viroid infected tissues (see above)— but also RISCs, seem to operate in containing viroid titer below certain levels.

Deep sequencing confirms loading of vd-sRNA by the endogenous AGO1 of *N. benthamiana* infected by PSTVd. As a final control in an experimental context excluding agroexpression of AGO proteins from *A. thaliana*, we also performed a deep sequencing analysis of the vd-sRNAs in the input and IP generated by a polyclonal antibody against the endogenous AGO1 from PSTVd-infected *N. benthamiana* (Fig. 1C). The analysis of the two bar-coded samples run in the same channel resulted in 3.839.392 reads of 18-26 nt vd-sRNAs (8.5% of total reads of the input) and 4.270.376 reads of 18-26 nt vd-sRNA (9.3% of total reads of the IP). While the proportion of vd-sRNAs of 21, 22 and 24 nt in the input were similar (27-32%), the 21- and 22-nt vd-sRNAs in the IP amounted to 63 and 28%, respectively, with those of 24 nt only representing 2%. Therefore, AGO1 from *N. benthamiana* exerted a size selection on the vd-sRNAs similar to its homologue from *A. thaliana,* displaying a clear preference for binding those of 21 and (to lower extent) 22 nt. Regarding polarity, the (+) and (-) vd-sRNAs in the input represented 66 and 34%, respectively, while the ratio in the IP was reversed (39 and 61%, respectively). The size selection exerted by AGO1 from *N. benthamiana* on vd-sRNAs (see above) was not significantly influenced by their polarity.

An enrichment/depletion analysis of vd-sRNA reads in the IP versus the input showed a significant enrichment in the IP of (+) and (-) vd-sRNAs of 21 and 22 nt (but not of 24 nt) with a 5'-terminal U (but not with the three other 5'-terminal nucleotides) (Fig. 7). Therefore, regarding binding specificity for vd-sRNAs, AGO1 from *N. benthamiana* behaved similarly to its agroexpressed homologue from *A. thaliana.*

Finally, the profile of vd-sRNAs loaded by AGO1 from *N. benthamiana* presented a specific hot spot distribution along the viroid genome (Fig. 7 or 8), thus recapitulating the situation previously observed with the agroexpressed AGOs from *A. thaliana.* However, the vd-sRNA profiles corresponding to the agroinfiltrated AGO1 from *A. thaliana* and the endogenous AGO1 from *N. benthamiana* differed, most likely because of the different experimental conditions: in the first instance the AGO1

from *A. thaliana* was over-expressed, while in the second instance the accumulation of the endogenous AGO1 should be considerably lower and possibly subjected to developmental regulation.

DISCUSSION

Our first immunoprecipitation assays, using PSTVd-infected leaves of *N. benthamiana* and a polyclonal antibody specific for its endogenous AGO1, showed that this protein indeed binds preferentially vd-sRNAs with the expected size (21- 22 nt). However, PSTVd infection of *N. benthamiana* did not affect significantly the accumulation of either endogenous AGO1 or miR168 (which regulates AGO1 mRNA expression), as opposed to the situation observed in the same host following infection by different RNA viruses (42, 60). Considering that in the latter case the specific induction of miR168 is promoted by viral-encoded protein suppressors of RNA silencing, and that PSTVd is a non-protein coding RNA, this result is not surprising. Moreover, it does not either favor that vd-sRNAs, as proposed previously for transgene siRNAs and endogenous siRNAs and miRNAs (68), could compete to bind to AGO1 and lead to a reduction in AGO1-miR168 complexes and a decline in AGO1 mRNA cleavage. However, recent data indicate that infection by citrus exocortis viroid, a close relative of PSTVd, induces the accumulation of other enzymes mediating RNA silencing steps in tomato (69). Whether this accumulation is a direct or indirect effect, and which is the nature of the underlying mechanism, remains unknown.

Previous reports indicate that viroids are significantly resistant to RISC-mediated degradation (47, 70, 71), suggesting that they may have evolved their secondary structures as a response against this selection pressure. In such a scenario, the compact secondary structure of PSTVd (+) strands may hinder their targeting (and inactivation) by AGO proteins loaded with vd-sRNAs, being even more difficult targeting PSTVd (-) strands because they mostly form part of double-stranded

replicative complexes (8). From an alternative perspective, the secondary structure of viroids could have emerged as a compromise between resistance to DCL and RISC, which act preferentially against RNAs with compact and relaxed conformations, respectively (48). Indeed, data obtained in other experimental contexts indicate that viroids are RISC-sensitive (46, 48, 49, 52), and recent results show that RISC promotes cleavage of viral RNAs with a packed secondary structure —resembling that of viroids— by targeting bulged regions within this structure (72). However, the evidence that one or more AGOs are loaded with vd-sRNAs and function in antiviroid RISC is circumstantial, with no data providing direct support for this view.

The finding in tissues infected by typical members of both viroid families of vd-sRNAs with the characteristic features of DCL products (see above), does not necessarily entail their loading in one or more AGO proteins. Previous data from a study with an RNA virus have shown that the bulk of virus-derived sRNAs in latently infected Drosophila cells are not loaded into any AGO member, suggesting that dicing of viral dsRNAs, by itself, plays a key function in maintaining the latent state (73). Although dicing of the snap-folded genomic viroid ssRNA (or, more likely, of its dsRNA replication intermediates) could play a role in containing infection below a threshold value, extension of the "dicing-only" model to PSTVd does not seem justified. In support of this view, when nine of the ten AGOs from *A. thaliana* were agroexpressed in PSTVd-infected leaves of *N. benthamiana* all, except AGO6, AGO7 and AGO 10, bound vd-sRNAs: AGO1, AGO2 and AGO3 those of 21 and 22 nt, while AGO4, AGO 5 and AGO9 bound additionally those of 24 nt. Deep sequencing showed that, when agroexpressed in PSTVd-infected *N. benthamiana* leaves, AGO1, AGO2, AGO4 and AGO5 bound the vd-sRNA, particularly those of 21 and 22 nt, primarily according to their 5'-terminal nucleotide, as reported previously for endogenous and viral sRNAs (34, 35, 63). Moreover, the ratio of vd-sRNA to total sRNAs in the AGO-IPs was higher than that in the inputs, indicating that vd-sRNA were loaded into these AGO proteins even with some preference. Therefore, DCLs could function as the first

defense barrier against viroid infection and, additionally, provide vd-sRNAs for priming the second RISC-based defensive barrier.

Viroids, lacking protein-coding ability, might have also evolved a sort of RNA-mediated decoy mechanism protecting them against RNA silencing similar to that developed by alphaviruses, like Semliki forest virus (SFV), which neither encode RNA silencing suppressors. More specifically, alphaviruses have been proposed to produce decoy virus-derived sRNAs to hamper the RNA silencing machinery and to provide time to the virus for replication before being eventually silenced (74). In consonance with this view, the predominant virus sRNAs derived from hot spots are less effective at silencing SFV accumulation than those derived from cold spots (74). Regarding viroids, infections by PSTVd and the chloroplast-replicating peach latent mosaic viroid (PLMVd) (75), are accompanied by large amounts of vd-sRNAs (44, 45; this work). Moreover, the experimental evidence available supports that vd-sRNAs, mapping at cold spots, are biologically active. Specifically, variants of PLMVd inducing a severe albinism have a particular hairpin insertion of 12-14 nt (76, 77), and two low-abundant (-) vd-sRNAs containing this insertion target for cleavage —as predicted by RNA silencing— the peach mRNA coding for cHSP90 involved in plastid-to-nucleus signal transduction (51). The two vd-sRNAs are of 21-nt, fulfill the criteria for being functional sRNAs (78, 79), and have a 5'-terminal U indicating that they are most likely loaded in AGO1; these criteria are also met by a 22-nt RNA, which contains the region responsible for the yellow phenotype incited by the Y satellite RNA of CMV and directs cleavage, via RNA silencing, of the mRNA of a gene involved in chlorophyll biosynthesis (80, 81). A similar mechanism has been proposed for the phenotypes induced by artificial miRNAs (amiRNAs) derived from the virulence-modulating region of PSTVd (82), although the evidence is indirect and the amiRNAs do not fulfill all the above-mentioned criteria. The finding that host mRNAs are targeted by AGOs loaded with sRNAs derived from viroids and satellite RNAs, supports that these subviral replicons, like RNA viruses, are also targets of RISC.

Previously, hypomorphic *ago1* mutants have been tested against virus infection, with their hypersensitive reaction and overaccumulation of viral RNA being interpreted as a confirmation of the involvement of RNA silencing, and particularly of AGO1, in antiviral defense (31). Here we have taken the opposite approach: to overexpress certain AGO proteins and examine whether they result in viroid underaccumulation. Specifically, the synchronized overexpression of AGO1, AGO2, AGO4 and AGO5 in leaves of *N. benthamiana* at early stages of PSTVd infection has facilitated the observation of the attenuating effects of these proteins on viroid titer. These results, together with the specific loading of vd-sRNAs of the expected size and 5'-terminal nucleotide by agroinfiltrated AGO1, AGO2, AGO4 and AGO5 from *A. thaliana,* as well as by the endogenous AGO1 of *N. benthamiana,* are consistent with the view that those members of the AGO family may play a role in anti-PSTVd defense.

ACKNOWLEDGEMENTS

We are grateful to Drs. A. Takeda and Y. Watanabe for kindly providing *35S:HA-AGO3*, *35S:HA-AGO4*, *35S:HA-AGO5*, *35S:HA-AGO6*, *35S:HA-AGO8* and *35S:HA-AGO9* constructs, to Dr. N. Fahlgren for helping in developing scripts for the deep sequencing analyses, to Dr. M. Cambra for a rabbit preimmune serum, to Dr. J. Burgyan for a rabbit polyclonal antibody against the N-terminal region of AGO1 from *N. benthamiana* that we used in preliminary experiments, and to A. Ahuir for excellent technical assistance. Research in R.F. laboratory is currently funded by grant BFU2011-28443 from the Ministerio de Economía y Competitividad (MINECO, Spain). S.M. has been supported by a fellowship and a predoctoral contract from MINECO. Research in B.N. and F.D.S. laboratory has been funded by the a dedicated grant of the Ministero dell'Economia e Finanze Italiano to the CNR (CISIA, Legge n. 191/2009). Research in J.C.C. laboratory was supported by grants from the National Science

Foundation (MCB-0956526, MCB-1231726) and National Institutes of Health (AI043288).

REFERENCES

1. **Flores R, Hernández C, Martínez de Alba AE, Daròs JA, Di Serio F.** 2005. Viroids and viroid-host interactions. Annu. Rev. Phytopathol. **43**:117-139.
2. **Tsagris EM, Martínez de Alba AE, Gozmanova M, Kalantidis K.** 2008. Viroids. Cell Microbiol. **10**:2168–2179.
3. **Ding B.** 2009. The biology of viroid-host interactions. Annu. Rev. Phytopathol. **47**:105-131.
4. **Diener TO.** 1967. Potato spindle tuber virus: A plant virus with properties of a free nucleic acid. Science **158**:378-381.
5. **Gross HJ, Domdey H, Lossow C, Jank P, Raba M, Alberty H, Sänger HL.** 1978. Nucleotide sequence and secondary structure of potato spindle tuber viroid. Nature **273**:203-208.
6. **Grill LK, Semancik JS.** 1978. RNA sequences complementary to citrus exocortis viroid in nucleic acid preparations from infected *Gynura aurantiaca.* Proc. Natl. Acad. Sci. U.S.A. **75**:896-900.
7. **Ishikawa M, Meshi T, Ohno T, Okada Y, Sano T, Ueda I, Shikata E.** 1984. A revised replication cycle for viroids: the role of longer than unit RNA in viroid replication. Mol. Gen. Gen. **196**:421-428.
8. **Branch AD, Benenfeld BJ, Robertson HD.** 1988. Evidence for a single rolling circle in the replication of potato spindle tuber viroid. Proc. Natl. Acad. Sci. U.S.A. **85**:9128-9132.
9. **Feldstein PA, Hu Y, Owens RA.** 1998. Precisely full length, circularizable, complementary RNA: an infectious form of potato spindle tuber viroid. Proc. Natl. Acad. Sci. U.S.A. **95**:6560-6565.
10. **Daròs JA, Flores R.** 2004. Arabidopsis thaliana has the enzymatic machinery for replicating representative viroid species of the family Pospiviroidae. Proc. Natl. Acad. Sci. U. S. A. **101**:6792-6797.

11. **Mühlbach HP, Sänger HL.** 1979. Viroid replication is inhibited by α-amanitin. Nature **278**:185-188.
12. **Flores R, Semancik JS.** 1982. Properties of a cell-free system for synthesis of citrus exocortis viroid. Proc. Natl. Acad. Sci. U.S.A. **79**:6285-6288.
13. **Schindler IM, Mühlbach HP.** 1992. Involvement of nuclear DNA-dependent RNA polymerases in potato spindle tuber viroid replication: a reevaluation. Plant Sci. **84**:221-229.
14. **Gas ME, Hernández C, Flores R, Daròs JA.** 2007. Processing of nuclear viroids *in vivo:* an interplay between RNA conformations. PLoS Pathog. **3**:1813-1826.
15. **Nohales MA, Flores R, Daròs JA.** 2012. Viroid RNA redirects host DNA ligase 1 to act as an RNA ligase. Proc. Natl. Acad. Sci. U.S.A. **109**:13805-13810.
16. **Gas ME, Molina-Serrano D, Hernández C, Flores R, Daròs JA.** 2008. Monomeric linear RNA of citrus exocortis viroid resulting from processing *in vivo* has 5′-phosphomonoester and 3′-hydroxyl termini: implications for the ribonuclease and RNA ligase involved in replication. J. Virol. **82**:10321-10325.
17. **Flores R, Daròs JA, Hernández C.** 2000. The *Avsunviroidae* family: viroids with hammerhead ribozymes. Adv. Virus Res. **55**:271-323.
18. **Qi Y, Pélissier T, Itaya A, Hunt E, Wassenegger M, Ding B.** 2004. Direct role of a viroid RNA motif in mediating directional RNA trafficking across a specific cellular boundary. Plant Cell **16**:1741-1752.
19. **Zhong X, Tao X, Stombaugh J, Leontis N, Ding B.** 2007. Tertiary structure and function of an RNA motif required for plant vascular entry to initiate systemic trafficking. EMBO J. **26**:3836-3846.
20. **Takeda R, Petrov AI, Leontis NB, Ding B.** 2011. A three-dimensional RNA motif in potato spindle tuber viroid mediates trafficking from palisade mesophyll to spongy mesophyll in *Nicotiana benthamiana.* Plant Cell **23**:258-272.
21. **Zhong X., Archual AJ, Amin AA, Ding B.** 2008. A genomic map of viroid RNA motifs critical for replication and systemic trafficking. Plant Cell **20**:35-47.

22. **Carthew RW, Sontheimer EJ.** 2009. Origins and mechanisms of miRNAs and siRNAs. Cell **136**:642-655.
23. **Ding SW.** 2010. RNA-based antiviral immunity. Nat. Rev. Immunol. **10**:632-644.
24. **Axtell MJ.** 2013. Classification and comparison of small RNAs from plants. Annu. Rev. Plant Biol. **64**:137-159.
25. **Incarbone M, Dunoyer P.** 2013. RNA silencing and its suppression: novel insights from in planta analyses. Trends Plant Sci. **18**:382-392.
26. **Pumplin N, Voinnet O.** 2013. RNA silencing suppression by plant pathogens: defence, counter-defence and counter-counter-defence. Nat. Rev. Microbiol. **11**:745-760.
27. **Schiebel W., Pélissier T, Riedel L, Thalmeir S, Schiebel R, Kempe D, Lottspeich F, Sänger HL, Wassenegger M.** 1998. Isolation of an RNA-directed RNA polymerase-specific cDNA clone from tomato. Plant Cell **10**:2087-2101.
28. **Voinnet O.** 2008. Use, tolerance and avoidance of amplified RNA silencing by plants. Trends Plant Sci. **13**:317-328.
29. **Mallory A, Vaucheret H.** 2010. Form, function, and regulation of ARGONAUTE proteins. Plant Cell **22**:3879-3889.
30. **Bologna NG, Voinnet O.** 2014. The diversity, biogenesis, and activities of endogenous silencing small RNAs in Arabidopsis. Annu. Rev. Plant Biol. **65**:473-503.
31. **Morel JB, Godon C, Mourrain P, Béclin C, Boutet S, Feuerbach F, Proux F, Vaucheret H.** 2002. Fertile hypomorphic ARGONAUTE (ago1) mutants impaired in post-transcriptional gene silencing and virus resistance. *Plant Cell* **14**:629-639.
32. **Baumberger N, Baulcombe DC.** 2005. Arabidopsis ARGONAUTE1 is an RNA slicer that selectively recruits microRNAs and short interfering RNAs. Proc. Natl. Acad. Sci. U.S.A. **102**:11928-11933.
33. **Qu F, Ye X, and Morris TJ.** 2008. *Arabidopsis* DRB4, AGO1, AGO7, and RDR6 participate in a DCL4-initiated antiviral RNA silencing pathway negatively regulated by DCL1. Proc. Natl. Acad. Sci. U.S,A, **105**:14732-14737.

34. **Montgomery TA, Howell MD, Cuperus JT, Li D, Hansen JE, AL Alexander, Chapman EJ, Fahlgren N, Allen E, Carrington JC.** 2008. Specificity of ARGONAUTE7-miR390 interaction and dual functionality in TAS3 trans-acting siRNA formation. Cell **133**:128-141.

35. **Takeda A, Iwasaki S, Watanabe T, Utsumi M, Watanabe Y.** 2008. The mechanism selecting the guide strand from small RNA duplexes is different among Argonaute proteins. Plant Cell Physiol. **49**:493-500.

36. **Alvarado VY, Scholthof HB.** 2011. AGO2: a new Argonaute compromising plant virus accumulation. Front. Plant Sci. **2**:article 112.

37. **Carbonell A, Fahlgren N, García-Ruiz H, Gilbert KB, Montgomery TA, Nguyen T, Cuperus JT, Carrington JC.** 2012. Functional analysis of three Arabidopsis ARGONAUTES using slicer-defective mutants. Plant Cell **24**:3613-3629.

38. **Zilberman D, Cao X, Jacobsen SE.** 2003. ARGONAUTE4 control of locus-specific siRNA accumulation and DNA and histone methylation. Science **299**:716-719.

39. **Havecker ER, Wallbridge LM, Hardcastle TJ, Bush MS, Kelly KA, Dunn RM, Schwach F, Doonan JH, Baulcombe DC.** 2010. The Arabidopsis RNA-directed DNA methylation argonautes functionally diverge based on their expression and interaction with target loci. Plant Cell **22**:321-334.

40. **Qi Y, He X, Wang XJ, Kohany O, Jurka J, Hannon GJ.** 2006. Distinct catalytic and non-catalytic roles of ARGONAUTE4 in RNA-directed DNA methylation. Nature **443**:1008-1012.

41. **Mallory AC, Hinze A, Tucker MR, Bouché N, Gasciolli V, Elmayan T, Lauressergues D, Jauvion V, Vaucheret H, Laux T.** 2009. Redundant and specific roles of the ARGONAUTE Proteins AGO1 and ZLL in development and small RNA-directed gene silencing. PLoS Genet **5**:e1000646.

42. **Várallyay E., Valoczi A, Agyi A, Burgyán J, Havelda Z.** 2010. Plant virus-mediated induction of miR168 is associated with repression of ARGONAUTE1 accumulation. EMBO J. **29**:3507–3519.

43. **Nakasugi K., Crowhurst RN, Bally J, Wood CC, Hellens RP, Waterhouse PM.** 2013. De novo transcriptome sequence assembly and analysis of RNA silencing genes of *Nicotiana benthamiana.* PLoS One **8**:e59534.

44. **Navarro B, Gisel A, Rodio ME, Delgado S, Flores R, Di Serio F**. 2012. Viroids: how to infect a host and cause disease without encoding proteins. Biochimie **94**:1474-1480.

45. **Hammann C, Steger G.** 2012. Viroid-specific small RNA in plant disease. RNA Biol. **9**:809-819.

46. **Vogt U, Pelissier T, Putz A, Razvi F, Fischer R, Wassenegger M.** 2004. Viroid-induced RNA silencing of GFP-viroid fusion transgenes does not induce extensive spreading of methylation or transitive silencing. Plant J. **1**:107-118.

47. **Itaya A, Zhong X, Bundschuh R, Qi Y, Wang Y, Takeda R, Harris AR, Molina C, Nelson RS, Ding B.** 2007. A structured viroid RNA is substrate for Dicer-like cleavage to produce biologically active small RNAs but is resistant to RISC-mediated degradation. J. Virol. **81**:2980-2994.

48. **Carbonell A, Martínez de Alba AE, Flores R, Gago S.** 2008. Double-stranded RNA interferes in a sequence-specific manner with infection of representative members of the two viroid families. Virology **371**:44-53

49. **Schwind N, Zwiebel M, Itaya A, Ding B, Wang MB, Krczal G, Wassenegger M.** 2009. RNAi-mediated resistance to potato spindle tuber viroid in transgenic tomato expressing a viroid hairpin RNA construct. Mol. Plant Pathol. **10**:459-469.

50. **Di Serio F, Martínez de Alba AE, Navarro B, Gisel A, Flores R.** 2010. RNA-dependent RNA polymerase 6 delays accumulation and precludes meristem invasion of a nuclear-replicating viroid. J. Virol. **84**:2477-2489.

51. **Navarro B, Gisel A, Rodio ME, Delgado S, Flores R, Di Serio F**. 2012. Small RNAs containing the pathogenic determinant of a chloroplast-replicating viroid guide the degradation of a host mRNA as predicted by RNA silencing. Plant J. **70**:991-1003.

52. **Serra P, Bani-Hashemian SM, Fagoaga C, Romero J, Ruiz-Ruiz S, Gorris MT, Bertolini E, Duran-Vila N.** 2014. Virus-viroid interactions: citrus tristeza virus enhances the accumulation of citrus dwarfing viroid in Mexican lime via the viral-encoded silencing suppressors. J. Virol. 88:1394-1397.
53. **Wassenegger M, Heimes S, Riedel L, Sänger HL.** 1994. RNA-directed de novo methylation of genomic sequences in plants, Cell **76**:567-576.
54. **Martínez G, Castellano M, Tortosa M, Pallás V, Gómez G.** 2014. A pathogenic non-coding RNA induces changes in dynamic DNA methylation of ribosomal RNA genes in host plants. Nucleic Acids Res. **42**:1553-1562.
55. **Grimsley N, Hohn B, Hohn T, Walden R.** 1986. Agroinfection, an alternative route for viral-infection of plants by using the Ti plasmid. Proc. Natl. Acad. Sci. U.S.A. **83**:3282-3286.
56. **Llave C, Xie Z, Kasschau KD, Carrington JC.** 2002. Cleavage of Scarecrow-like mRNA targets directed by a class of Arabidopsis miRNA. Science **297**:2053-2056.
57. **Cuperus JT, Carbonell A, Fahlgren N, Garcia-Ruiz H, Burke RT, Takeda A, Sullivan CM, Gilbert SD, Montgomery TA, Carrington JC.** 2010. Unique functionality of 22-nt miRNAs in triggering RDR6-dependent siRNA biogenesis from target transcripts in Arabidopsis. Nat. Struct. Mol. Biol. **17**:997-1003.
58. **Sambrook J, Fritsch EF, Maniatis T.** 1989. Molecular cloning: A Laboratory Manual, 2nd edn. Cold Spring Harbor Laboratory Press, Cold Spring Harbor, NY.
59. **Langmead B, Trapnell C, Pop M, Salzberg SL.** 2009. Ultrafast and memory-efficient alignment of short DNA sequences to the human genome. Genome Biology **10:**R25.
60. **Várallyay E, Havelda Z.** 2013. Unrelated suppressors of RNA silencing mediate the control of ARGONAUTE1 level. Mol. Plant Pathol. **14**:567-575.
61. **Mallory AC, Vaucheret H.** 2009. ARGONAUTE 1 homeostasis invokes the coordinate action of the microRNA and siRNA pathways. EMBO Rep. **10**:521-526.
62. **Matousek J, Kozlová P, Orctová L, Schmitz A, Pesina K, Bannach O, Diermann N, Steger G, Riesner D.** 2007. Accumulation of viroid-specific small RNAs and

increase of nucleolytic activities linked to viroid-caused pathogenesis. Biol. Chem. **388**:1-13.

63. **Mi S, Cai T, Hu Y, Chen Y, Hodges E, Ni F, Wu L, Li S, Zhou H, Long C, Chen S, Hannon GJ, Qi Y.** 2008. Sorting of small RNAs into Arabidopsis argonaute complexes is directed by the 5' terminal nucleotide. Cell **133**:116-127.
64. **Ho T, Wang H, Palletta D, Dalmay T.** 2007. Evidence for targeting common siRNA hotspots and GC preference by plant Dicer-like proteins FEBS Lett. **581**:3267-3272.
65. **Zhang Y, Chenghuan Y, Hanhui K.** 2014. GC content fluctuation around plant small RNA-generating sites. FEBS Lett. **588**:764-769.
66. **Qi Y, Ding B.** 2003. Inhibition of cell growth and shoot development by a specific nucleotide sequence in a noncoding viroid RNA. Plant Cell **15**:1360-1374.
67. **Schnölzer M, Haas B, Ramm K, Hofmann H, Sänger HL.** 1985. Correlation between structure and pathogenicity of potato spindle tuber viroid (PSTV). EMBO J. **4**:2181-2190.
68. **Martínez de Alba AE, Jauvion V, Mallory AC, Bouteiller N, Vaucheret H.** 2011. The miRNA pathway limits AGO1 availability during siRNA-mediated PTGS defense against exogenous RNA. Nucleic Acids Res. **39**:9339- 9344.
69. **Campos L, Granell P, Tárraga S, López-Gresa P, Conejero V, Bellés JM, Rodrigo I, Lisón P.** 2014. Salicylic acid and gentisic acid induce RNA silencing-related genes and plant resistance to RNA pathogens. Plant Physiol. Biochem. **77**:35-43.
70. **Wang MB, Bian XY, Wu LM, Liu LX, Smith NA, Isenegger D, RM Wu, Masuta C, Vance VB, Watson JM, Rezaian A, Dennis ES, Waterhouse PM.** 2004. On the role of RNA silencing in the pathogenicity and evolution of viroids and viral satellites. Proc. Natl. Acad. Sci. U.S.A. **101**:3275-3280.
71. **Gómez G, Pallás V.** 2007. Mature monomeric forms of hop stunt viroid resist RNA silencing in transgenic plants. Plant J. **51**:1041-1049.

72. **Schuck J, Gursinsky T, Pantaleo V, Burgyan J, Behrens SE.** 2013. AGO/RISC-mediated antiviral RNA silencing in a plant in vitro system. Nucleic Acids Res. **41**:5090-50103.

73. **Flynt A, Liu N, Martin R, Lai EC**. 2009. Dicing of viral replication intermediates during silencing of latent Drosophila viruses. Proc. Natl. Acad. Sci. U. S. A. **106**:5270-5275.

74. **Siu RW, Fragkoudis R, Simmonds P, Donald CL, Chase-Topping ME, Barry G, Attarzadeh-Yazdi G, Rodriguez-Andres J, Nash AA, Merits A, Fazakerley JK, Kohl A.** 2011. Antiviral RNA interference responses induced by Semliki Forest virus infection of mosquito cells: characterization, origin, and frequency-dependent functions of virus-derived small interfering RNAs. J. Virol. **85**:2907-2917.

75. **Hernández C, Flores R.** 1992. Plus and minus RNAs of peach latent mosaic viroid self-cleave in vitro via hammerhead structures. Proc. Natl. Acad. Sci. U.S.A. **89**:3711-3715.

76. **Malfitano M, Di Serio F, Covelli L, Ragozzino A, Hernández C, Flores R.** 2003. Peach latent mosaic viroid variants inducing peach calico contain a characteristic insertion that is responsible for this symptomatology. Virology **313**:492-501.

77. **Rodio ME, Delgado S, De Stradis AE, Gómez MD, Flores R, Di Serio F.** 2007. A viroid RNA with a specific structural motif inhibits chloroplast development. Plant Cell **19**:3610-3626.

78. **Iwakawa HO, Tomari Y.** 2013. Molecular insights into microRNA-mediated translational repression in plants. Mol Cell **52**:591-601.

79. **Liu Q, Wang F, Axtell MJ.** 2014. Analysis of complementarity requirements for plant microRNA targeting using a *Nicotiana benthamiana* quantitative transient assay. Plant Cell **26**:741-753.

80. **Shimura H, Pantaleo V, Ishihara T, Myojo N, Inaba JI, Sueda K, Burgyán J, Masuta C.** 2011. A viral satellite RNA induces yellow symptoms on tobacco by targeting a gene involved in chlorophyll biosynthesis using the RNA silencing machinery. PLoS Pathog. **7**:e1002021.

81. **Smith NA, Eamens AL, Wang MB.** 2011. Viral small interfering RNAs target host genes to mediate disease symptoms in plants. PLoS Pathog. **7**:e1002022.

82. **Eamens AL, Smith NA, Dennis ES, Wassenegger M, Wang MB.** 2014. In *Nicotiana* species, an artificial microRNA corresponding to the virulence modulating region of potato spindle tuber viroid directs RNA silencing of a soluble inorganic pyrophosphatase gene and the development of abnormal phenotypes. Virology **450-451**:266-277.

LEGENDS TO FIGURES

Fig. 1. PSTVd infection of *N. benthamiana* has no significant effect on AGO1 or miR168 accumulation in the upper non-inoculated leaves **(A)** or in the agroinfiltrated leaves **(B)**. Western-blot analyses were performed with a rabbit polyclonal antibody against the N-terminal region of AGO1 from *N. benthamiana* (α-AGO1) and a goat anti-rabbit secondary antibody conjugated to horseradish peroxidase. Total proteins were separated by PAGE in 4-12% gels and equal loading was assessed by the intensity of the large subunit of Rubisco after staining with Ponceau S. Northern-blot hybridizations were carried out with a 5'-radiolabeled oligodeoxyribonucleotide complementary to miR168. Total RNAs were separated by denaturing PAGE in 17% gels and equal loading was assessed by the intensity of tRNA after staining with ethidium bromide. Samples in **(A)** were collected at 15 (lanes 1 and 5), 20 (lanes 2 and 6), 25 (lanes 3 and 7) and 30 (lanes 4 and 8) days post inoculation (dpi); samples in **(B)** were collected at four (lanes 1 and 4), 6 (lanes 2 and 5) and eight (lanes 3 to 6) dpi. **(C)** Endogenous AGO1 loads vd-sRNAs during PSTVd infection of *N. benthamiana*. Aliquots of total sRNA (INPUT) and of the sRNA fraction immunoprecipitated with a rabbit polyclonal antibody against the N-terminal region of AGO1 from *N. benthamiana* (IP), were separated by denaturing PAGE in 17% gels and revealed by Northern-blot hybridization with a radiolabeled riboprobe for detecting PSTVd (+) strands. Lanes 1 and 4 correspond to a mock-inoculated control, and lanes 2, 3, 5 and 6 to PSTVd-infected upper non-inoculated leaves collected at 25 days post inoculation. IPs were obtained with the antibody against AGO1 (α-AGO1) (lanes 4 and 6) or with a preimmune rabbit immunoglobuline fraction (IgG) (lane 5). Mock inoculations were performed with cultures of *A. tumefaciens* with a binary plasmid expressing GUS intead of the head-to-tail dimeric (+) transcript of PSTVd. Accumulation of the PSTVd *mc* and *ml* forms was also examined in the RNA Inputs after denaturing PAGE in 5% gels (upper panel). Equal loading was assessed by the

intensity of the bands generated by the 5S and tRNAs after staining with ethidium bromide.

Fig. 2. (A) AGO1 and AGO2, but neither AGO7 nor AGO10, bind specifically certain vd-sRNAs. Northern-blot hybridizations with a full-length radiolabeled riboprobe for detecting PSTVd (+) strands of total RNAs (INPUT) from mock- and PSTVd-inoculated *N. benthamiana* agroinfiltrated with cultures of *A. tumefaciens* with binary plasmids for expressing HA-tagged AGO1 (lanes 1 and 2), AGO2 (lane 3), AGO7 (lanes 7 and 9) and AGO10 (lane 11). A size marker was included in lane M. RNA immunoprecipitates (IP) generated with an anti-HA monoclonal antibody from the halos agroexpressing HA-tagged AGO1 (lanes 4 and 5), AGO 2 (lane 6), AGO7 (lanes 8 and 10) and AGO10 (lane 12) were similarly analyzed. **(B).** Other agroinfiltrated AGOs, apart from AGO1 and AGO2, bind also vd-sRNAs with different affinity. Northern-blot hybridizations with a full-length radiolabeled riboprobe for detecting PSTVd (+) strands of total RNAs (INPUT) from mock- and PSTVd-inoculated *N. benthamiana* agroinfiltrated with cultures of *A. tumefaciens* with binary plasmids for expressing HA-tagged AGO2 (lanes 1, 2, 9 and 10), AGO4 (lane 3), AGO5 (lane 4), AGO3 (lane 11), AGO6 (lane 12) and AGO9 (lane 13). RNA immunoprecipitates (IP) generated with an anti-HA monoclonal antibody from the halos agroexpressing HA-tagged AGO2 (lanes 5, 6, 14 and 15), AGO4 (lane 7), AGO5 (lane 8), AGO3 (lane 16, overexposed to make the band visible), AGO6 (lane 17) and AGO9 (lane 18) were similarly analyzed. RNAs were separated by denaturing PAGE in 17% gels, and equal loading was assessed by the intensity of tRNA after staining with ethidium bromide. Western-blot analyses of total proteins from halos were carried out with the anti-HA monoclonal antibody following protein separation by PAGE in 4-12% gels; equal loading was assessed by the intensity of the large subunit of Rubisco after staining with Ponceau S. Mock inoculations were performed with cultures of *A. tumefaciens* with a binary plasmid expressing GUS instead of the head-to-tail dimeric transcript of PSTVd. In all cases

samples were processed two days after agroinfiltration of plants that were PSTVd-infected, or mock-inoculated, 19 days before.

Fig. 3. Size distribution of PSTVd and plant sRNAs (orange and green, respectively) in total RNAs (INPUT) and immunoprecipitates (IP) from halos of PSTVd-infected *N. benthamiana* agroinfiltrated with cultures of *A. tumefaciens* with binary plasmids for expressing HA-tagged versions of AGO1, AGO2, AGO4 and AGO5 from *A. thaliana*. The histograms compare the distribution of 18–26-nt total sRNA reads. The IP fractions were generated with an anti-HA monoclonal antibody. Notice that the scales are not identical in the different histograms, and that the fraction of PSTVd-sRNAs could be higher considering that the viroid may not invade all cells.

Fig. 4. Sorting of PSTVd-sRNAs into AGO1, AGO2, AGO4 and AGO5 mainly depends on their 5′-terminal nucleotide. The histograms display, in total RNA (INPUT) and in RNA immunoprecipates (IP), the fraction (in %) of total reads corresponding to the 21–, 22- and 24-nt PSTV-sRNAs (panels **A, B** and **C,** respectively) with distinct 5′ termini.

Fig. 5. AGO-loaded vd-sRNAs adopt along the viroid genome hot spot distributions that are specific for each of the four HA-tagged AGO from *A. thaliana* agroexpressed in PSTVd-infected *N. benthamiana*. Location and frequency in the genomic PSTVd RNA of the 5′ termini of the plus-strand (positive values) and minus-strand (negative values) vd-sRNA reads per million (rpm) from total RNAs (INPUT) and from immunoprecìpitates (IP) generated with an anti-HA monoclonal antibody. **(A)** to **(D),** profiles corresponding to AGO1, AGO2, AGO4 and AGO5, respectively. Note that the same numbers are used in the plus polarity (5′ to 3′ orientation is from left to right) and in the minus polarity (5′ to 3′ orientation is from right to left).

Fig. 6. Agroexpression of AGO1, AGO2, AGO4 and AGO5, but neither of AGO7 nor of GUS, attenuates viroid accumulation. Northern-blot hybridizations with a full-length radiolabeled riboprobe for detecting PSTVd (+) strands of total RNAs from halos of mock- and PSTVd-inoculated *N. benthamiana* agroinfiltrated with cultures of *A. tumefaciens* with binary plasmids for expressing HA-tagged AGO1 (panel **A,** lanes 1, 4 and 5), AGO2 (panel **A,** lanes 6 and 7), AGO4 (panel **B,** lanes 1, 4 , 5 and 6), AGO5 (panel **B,** lanes 7, 8 and 9) and AGO7 (panel **A,** lanes 8 and 9, and panel **B,** lanes 10 and 11), and GUS (panels **A** and **B,** lanes 2 and 3). Mock inoculations were performed as indicated in the legend to Fig. 3. Total RNAs ~~from halos~~, extracted two days after agroinfiltration, were separated by denaturing PAGE in 5% gels, and equal loading was assessed by the intensity of tRNA after staining with ethidium bromide. Western-blot analyses of total proteins from halos were carried out with the anti-HA monoclonal antibody following protein separation by PAGE in 4-12% gels; equal loading was assessed by the intensity of the large subunit of Rubisco after staining with Ponceau S. In all cases samples were processed two days after agroinfiltration of plants that were PSTVd-infected, or mock-inoculated, eight days before.

Fig. 7. Analysis of vd-sRNAs in the IP versus the INPUT generated by a polyclonal antibody against AGO1 from *N. benthamiana* reveals a clear enrichment in the IP of (+) **(A)** and (-) **(B)** vd-sRNAs of 21 and 22 nt (but not of 24 nt) with a 5'-terminal U. IP enrichment or depletion was determined for each unique 21-, 22- or 24-nt vd-sRNA as $\log_2$ [(IP reads + 1)/(INPUT reads +1)], and plotted for each size class as the fraction (%) of unique vd-sRNA sequences enriched >2-fold ($\log_2$ >1) or depleted >2-fold ($\log_2$<1) in the IP compared.

Fig. 8. AGO1-loaded vd-sRNAs adopt along the viroid genome a hot spot distribution in PSTVd-infected *N. benthamiana*. Location and frequency in the genomic PSTVd RNA of the 5' termini of the plus-strand (positive values) and minus-strand (negative values) vd-sRNA reads per million (rpm) from total RNAs (INPUT, top panel) and from

the immunoprecipitate (IP, bottom panel) generated with an anti-*Nicotiana benthamiana* AGO1 (Nb AGO1) polyclonal antibody. Other details as in the legend to figure 5.

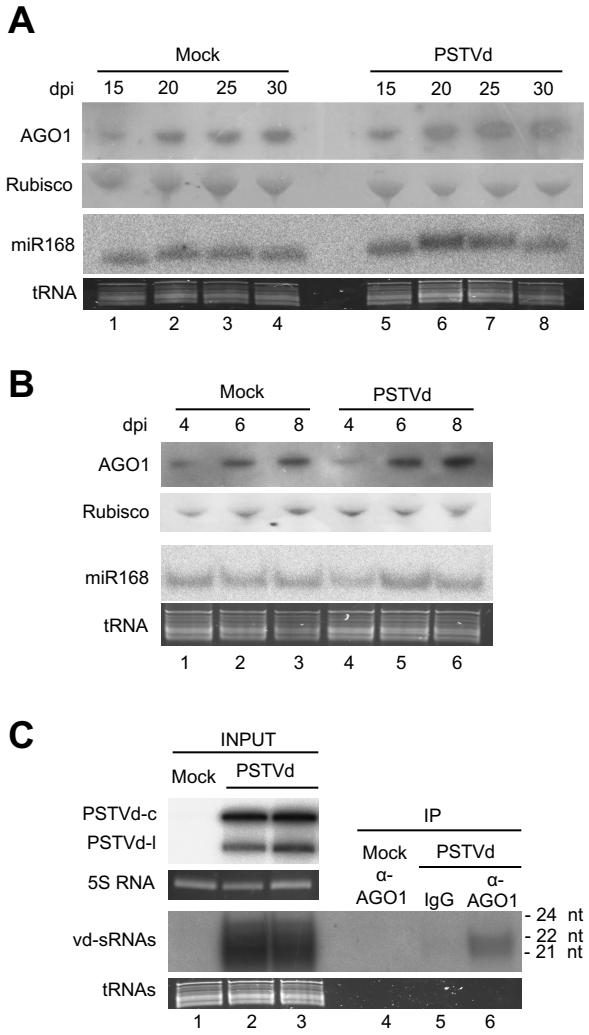
A
Mock
PSTVd
dpi
15
20
25
30
15
20
25
30
AGO1
Rubisco
miR168
tRNA
1
2
3
4
5
6
7
8
B
Mock
PSTVd
dpi
4
6
8
4
6
8
AGO1
Rubisco
miR168
tRNA
1
2
3
4
5
6
C
INPUT
Mock
PSTVd
PSTVd-c
PSTVd-l
5S RNA
IP
Mock
PSTVd
α-AGO1
IgG
α-AGO1
vd-sRNAs
- 24 nt
- 22 nt
- 21 nt
tRNAs
1
2
3
4
5
6

Figure 1

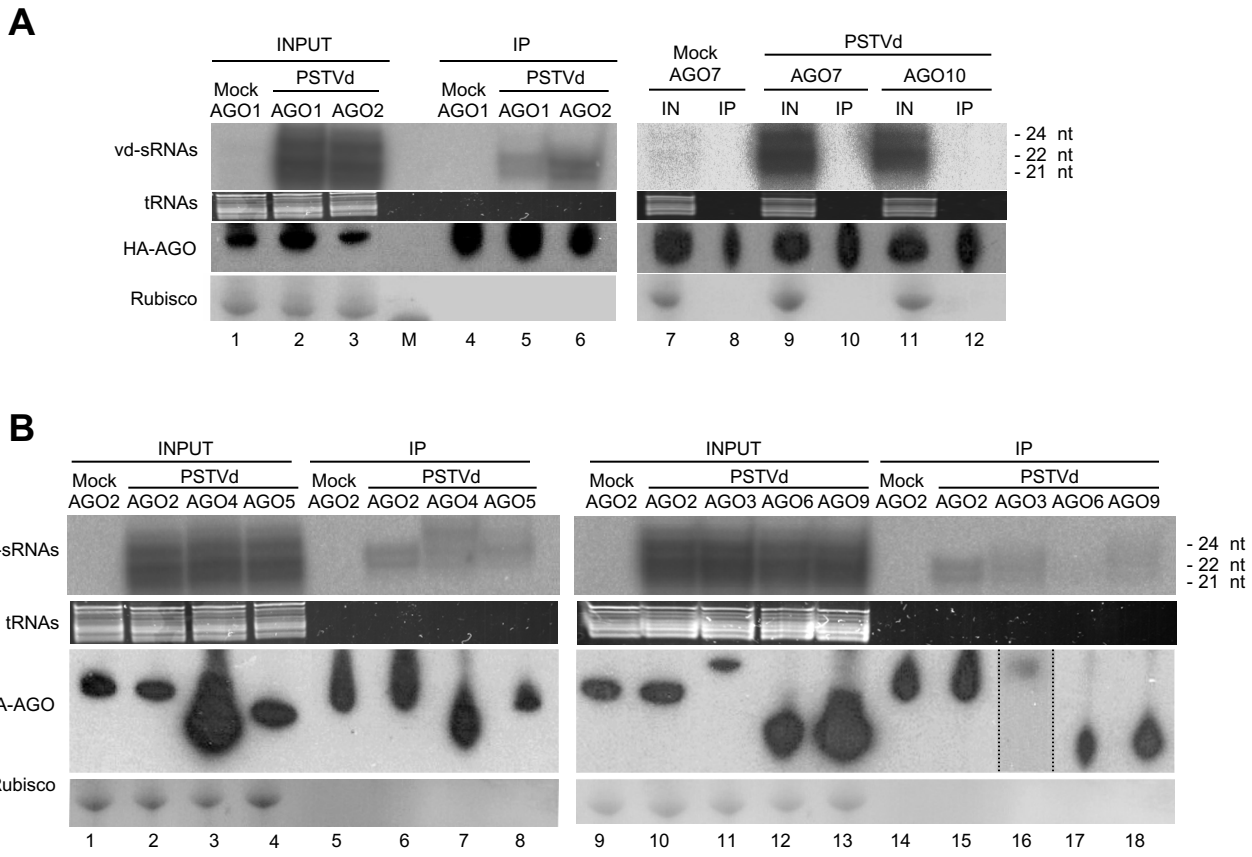
A
INPUT
IP
Mock
PSTVd
AGO1
AGO2
AGO7
AGO10
IN
IP
vd-sRNAs
tRNAs
HA-AGO
Rubisco
- 24 nt
- 22 nt
- 21 nt
1 2 3 M 4 5 6 7 8 9 10 11 12
B
AGO4
AGO5
AGO3
AGO6
AGO9
1 2 3 4 5 6 7 8 9 10 11 12 13 14 15 16 17 18

Figure 2

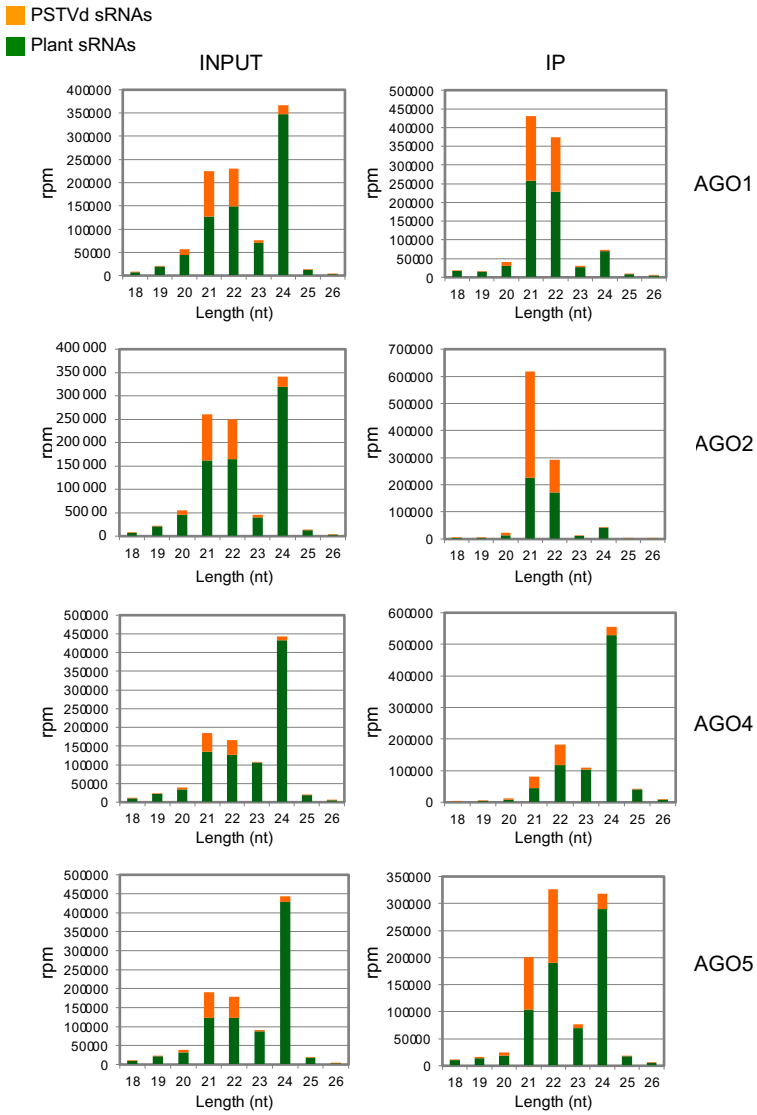
PSTVd sRNAs
Plant sRNAs
INPUT
IP
AGO1
AGO2
AGO4
AGO5
rpm
Length (nt)
18 19 20 21 22 23 24 25 26

Figure 3

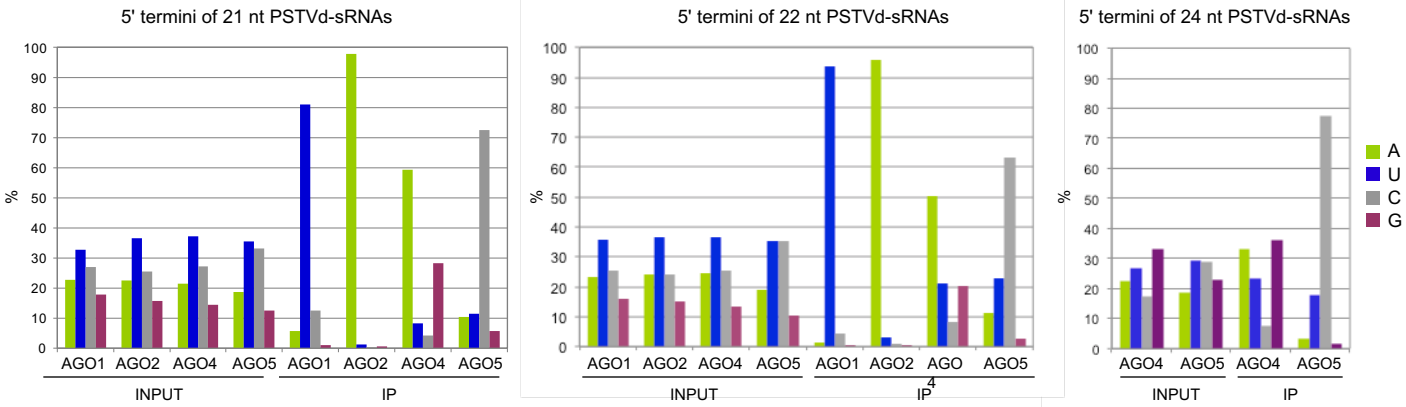
5' termini of 21 nt PSTVd-sRNAs
5' termini of 22 nt PSTVd-sRNAs
5' termini of 24 nt PSTVd-sRNAs
%
100
90
80
70
60
50
40
30
20
10
0
AGO1
AGO2
AGO4
AGO5
AGO
INPUT
IP
A
U
C
G

Figure 4

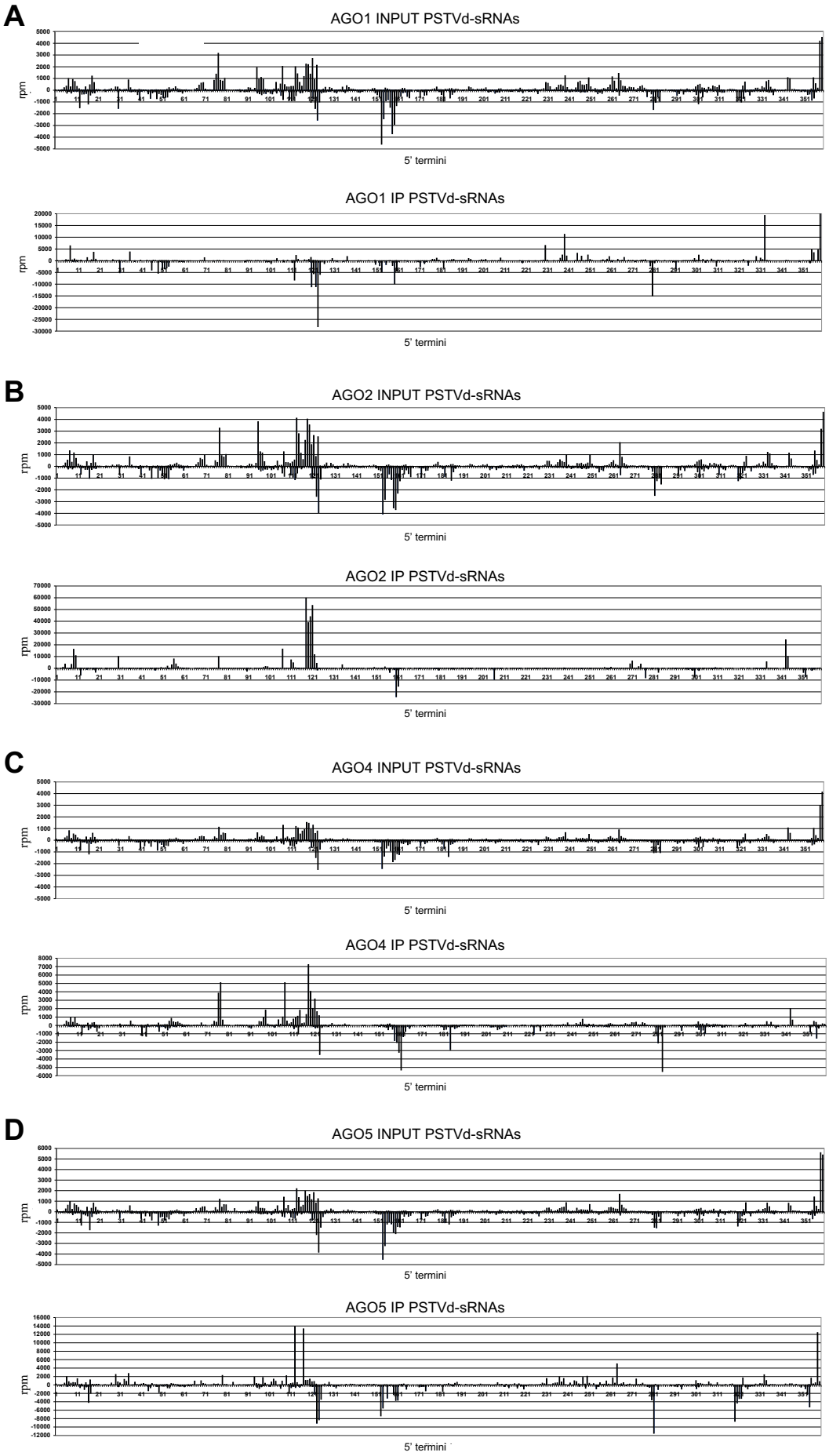
A
AGO1 INPUT PSTVd-sRNAs
rpm
5' termini
AGO1 IP PSTVd-sRNAs
rpm
5' termini
B
AGO2 INPUT PSTVd-sRNAs
rpm
5' termini
AGO2 IP PSTVd-sRNAs
rpm
5' termini
C
AGO4 INPUT PSTVd-sRNAs
rpm
5' termini
AGO4 IP PSTVd-sRNAs
rpm
5' termini
D
AGO5 INPUT PSTVd-sRNAs
rpm
5' termini
AGO5 IP PSTVd-sRNAs
rpm
5' termini

Figure 5

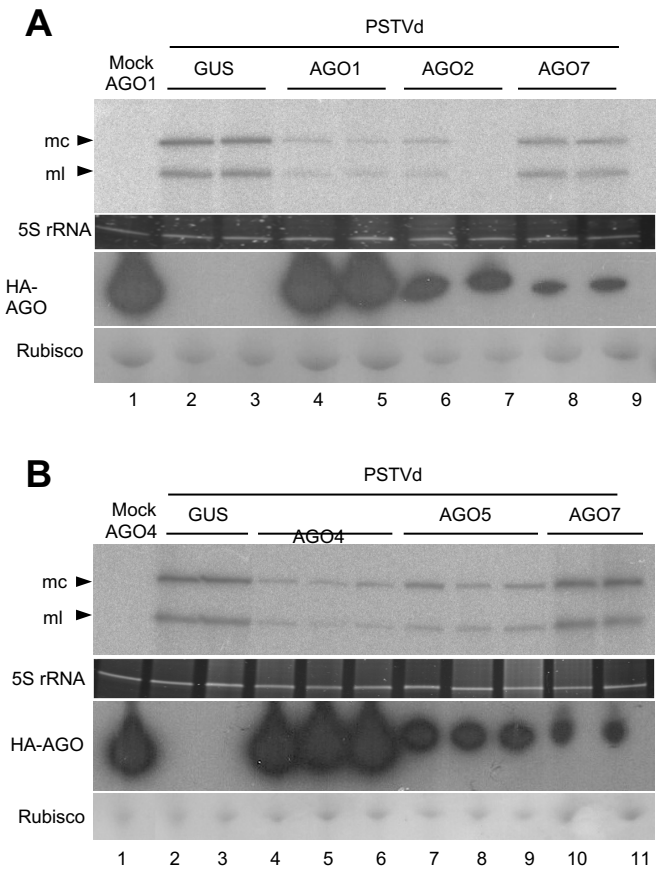
A
PSTVd
Mock
AGO1
GUS
AGO1
AGO2
AGO7
mc
ml
5S rRNA
HA-
AGO
Rubisco
1 2 3 4 5 6 7 8 9
B
PSTVd
Mock
AGO4
GUS
AGO4
AGO5
AGO7
mc
ml
5S rRNA
HA-AGO
Rubisco
1 2 3 4 5 6 7 8 9 10 11

Figure 6

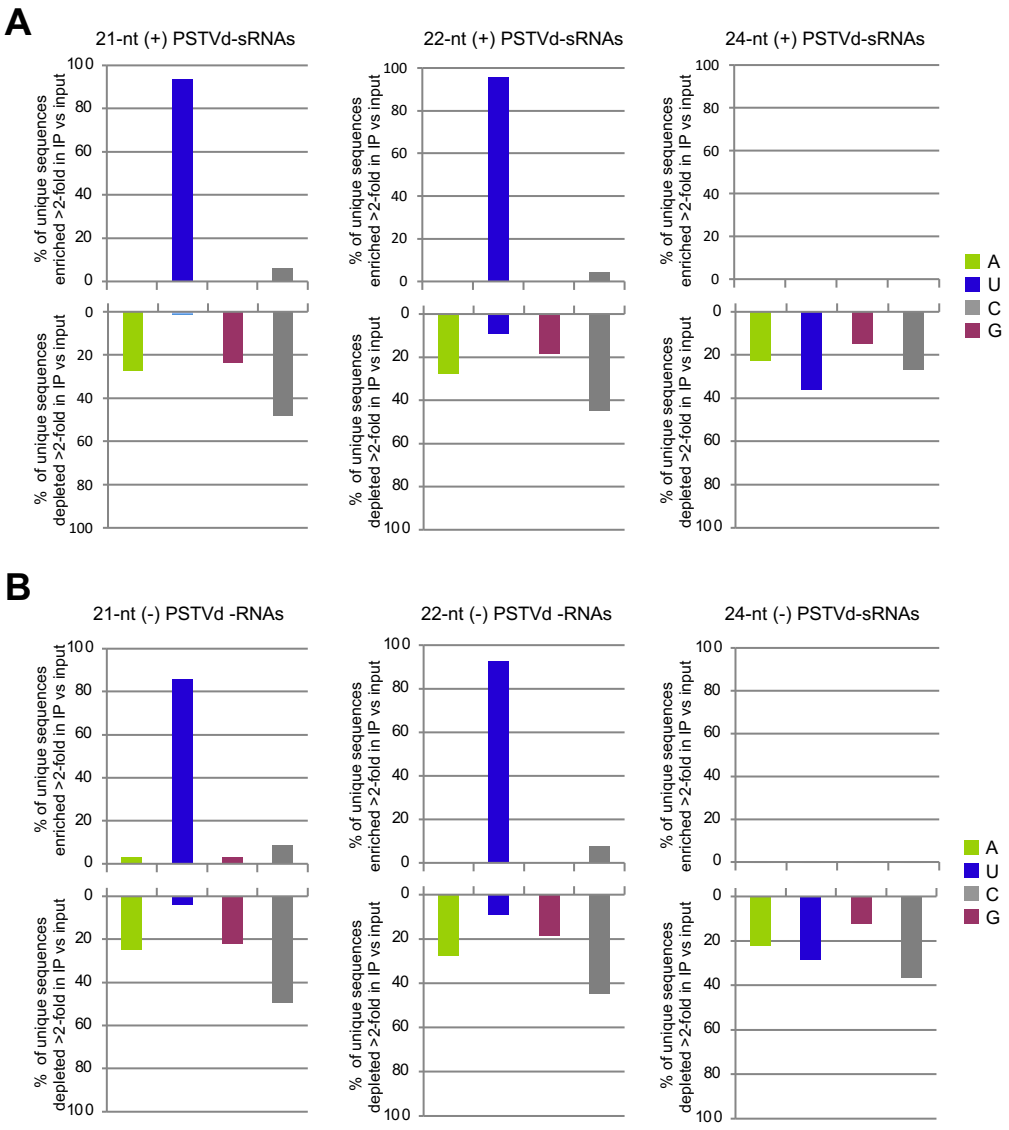
A
21-nt (+) PSTVd-sRNAs
22-nt (+) PSTVd-sRNAs
24-nt (+) PSTVd-sRNAs
% of unique sequences enriched >2-fold in IP vs input
% of unique sequences depleted >2-fold in IP vs input
100
80
60
40
20
0
A
U
C
G
B
21-nt (-) PSTVd -RNAs
22-nt (-) PSTVd -RNAs
24-nt (-) PSTVd-sRNAs

Figure 7

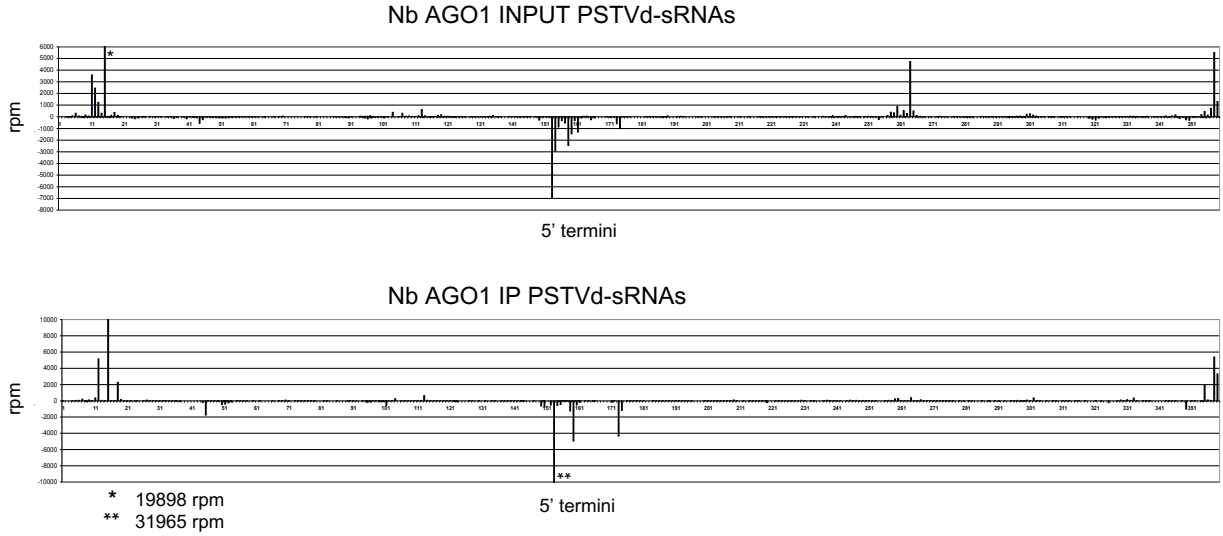

* 19898 rpm
** 31965 rpm

Figure 8